546 *Biochemistry* **2011,** *50,* 546–557
DOI: 10.1021/bi101776t

BIOCHEMISTRY
including biophysical chemistry & molecular biology
Article

Thermodynamic Characterization of the Binding Interaction between the Histone Demethylase LSD1/KDM1 and CoREST[†]

Sunhee Hwang, Allison A. Schmitt, Andrea E. Luteran, Eric J. Toone, and Dewey G. McCafferty*

Department of Chemistry, B120 Levine Science Research Center, Box 90317, Duke University, Durham, North Carolina 27708, United States

Received November 4, 2010; Revised Manuscript Received December 9, 2010

ABSTRACT: Flavin-dependent histone demethylases catalyze the posttranslational oxidative demethylation of mono- and dimethylated lysine residues, producing formaldehyde and hydrogen peroxide in addition to the corresponding demethylated protein. *In vivo*, histone demethylase LSD1 (KDM1; BCH110) is a component of the multiprotein complex that includes histone deacetylases (HDAC 1 and 2) and the scaffolding protein CoREST. Although little is known about the affinities of or the structural basis for the interaction between CoREST and HDACs, the structure of CoREST$^{286-482}$ bound to an α-helical coiled-coil tower domain within LSD1 has recently been reported. Given the significance of CoREST in directing demethylation to specific nucleosomal substrates, insight into the molecular basis of the interaction between CoREST and LSD1 may suggest a new means of inhibiting LSD1 activity by misdirecting the enzyme away from nucleosomal substrates. Toward this end, isothermal titration calorimetry studies were conducted to determine the affinity and thermodynamic parameters characterizing the binding interaction between LSD1 and CoREST$^{286-482}$. The proteins tightly interact in a 1:1 stoichiometry with a dissociation constant (K_d) of 15.9 ± 2.07 nM, and their binding interaction is characterized by a favorable enthalpic contribution near room temperature with a smaller entropic penalty at pH 7.4. Additionally, one proton is transferred from the buffer to the heterodimeric complex at pH 7.4. From the temperature dependence of the enthalpy change of interaction, a constant-pressure heat capacity change (ΔC_p) of the interaction was determined to be −0.80 ± 0.01 kcal mol^{-1} K^{-1}. Notably, structure-driven truncation of CoREST revealed that the central binding determinant lies within the segment of residues 293−380, also known as the CoREST "linker" region, which is a central isolated helix that interacts with the LSD1 coiled-coil tower domain to create a triple-helical bundle. Thermodynamic parameters obtained from the binding between LSD1 and the linker region of CoREST are similar to those obtained from the interaction between LSD1 and CoREST$^{286-482}$. These results provide a framework for understanding the molecular basis of protein−protein interactions that govern nucleosomal demethylation.

As part of the epigenetic regulation of gene expression, the structure of chromatin is influenced by association with nonhistone proteins or multiprotein complexes, the activity of multiprotein chromatin remodeling complexes, and protein complexes responsible for the posttranslational modification of histones. Protein−protein interactions govern many events in chromatin enzymology, especially those surrounding the site-specific posttranslational modification of histones at the level of individual nucleosomes. In the nucleosome, the basic unit of chromatin, ∼147 base pairs of DNA wind about a histone octamer that is composed of two copies each of histone proteins H2A, H2B, H3, and H4 (*1*, *2*). The highly conserved sequence of the N-terminal segment of each histone protein extends out of the nucleosome and provides sites for various posttranslational modifications, including acetylation, phosphorylation, ubiquitination, and methylation.

Posttranslational methylation of histones is a modification that has been intimately linked with both transcriptional activation and repression events; the context of these seemingly opposing activities depends on the type of histone being modified, the specific residue being modified, and the degree of mono-, di-, or trimethyl modification (*3*−*5*). Whereas the action of *S*-adenosylmethionine-dependent histone methyltransferases produces methylated histones, removal of methyl marks is performed by two classes of oxidative demethylation enzymes: flavin-dependent histone demethylases such as LSD1[1] and LSD2 (also known as KDM1/BCH110 and KDM2/AOF1, respectively) and Jumonji domain C (JmjC) family histone demethylases that utilize Fe(II) and α-ketoglutarate as cofactors.

Human LSD1 and LSD2 belong to the flavin adenine dinucleotide (FAD)-dependent family of amine oxidases, members of which include monoamine oxidase A, monoamine oxidase B, and polyamine oxidase (*3*, *6*). LSD1 selectively catalyzes the demethylation of mono- and dimethylated lysine 4 of histone H3 (H3K4) via the

[†]This work was generously supported by Grant RO1-GM087566 to D.G.M. from the National Institute of General Medical Sciences, and A.A.S. acknowledges support from the Duke Pharmacological Sciences Training Program, NIH T32-GM007105-37.

*To whom correspondence should be addressed. Phone: (919) 660-1516. Fax: (919) 668-5483. E-mail: dewey.mccafferty@duke.edu.

[1]Abbreviations: LSD1, lysine-specific demethylase 1; CoREST, corepressor to the silencer REST (RE1 silencing transcription factor/neural restrictive silencing factor); FPLC, fast protein liquid chromatography; KDM1, newly accepted nomenclature for the LSD1 histone demethylase; ITC, isothermal titration calorimetry; ΔH, enthalpy change; ΔS, entropy change; ΔC_p, constant-pressure heat capacity change; K_d, equilibrium dissociation constant; *n*, stoichiometry; K_a, equilibrium association constant.

 Published on Web 12/10/2010

Scheme 1: General Mechanism of Lysine Demethylation by LSD1

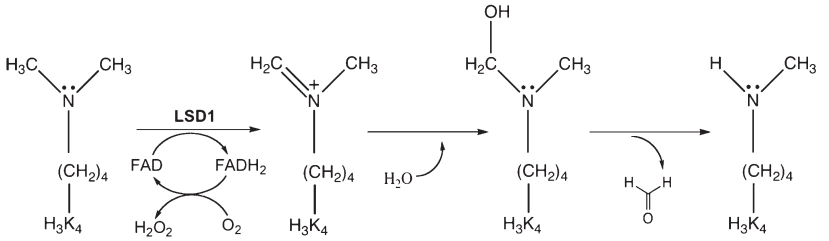

oxidative process outlined in Scheme 1. The mono- or dimethylated amine of lysine is oxidized with assistance from the oxidized FAD cofactor to form an imine intermediate that hydrolyzes to produce formaldehyde and the demethylated side chain on histone H3. In a final step, the flavin cofactor is reoxidized by molecular oxygen, forming hydrogen peroxide (*7*). Through this mechanism, LSD1 can demethylate mono- and dimethylated lysine but lacks the ability to demethylate trimethylated lysine.

As a result of this catalytic activity, LSD1 disrupts methylated histone modification and leads to repressed transcription (*4*), resulting in severe pathological consequences inducing cancer progression. LSD1 is consistently found in various transcriptional corepressor complexes that include CoREST, CtBP (C-terminal binding protein), and HDAC 1 and 2 (histone deacetylase 1 and 2, respectively) (*4*−*6*), indicating that LSD1 activity can be modulated by its interacting proteins. LSD1 has also been shown to interact with p53, a tumor suppressor gene, and repress p53-mediated transcription (*8*). Consequently, the upregulation of LSD1 has been related to an early response to carcinogen exposure in human mammalian epithelial cells (*9*), a high risk of prostate cancer (*10*), and breast carcinogenesis (*11*).

LSD1 alone is sufficient to demethylate H3K4 in peptides or bulk histones, but its activity toward nucleosomal substrates is regulated by its interaction with CoREST (*4*, *12*). CoREST is a 66 kDa protein that functions as a corepressor to the silencer REST (RE1 silencing transcription factor/neural restrictive silencing factor) (*12*, *13*). It consists of an ELM2 (Egl-27 and MTA1 homology 2) domain, two SANT (Swi3/Ada2/NCoR/transcription factor IIIB) domains, and the linker region between the two SANT domains (Figure 1). Recent studies have shown that the C-terminal fragment of CoREST (residues 286−482, abbreviated CoREST$^{286-482}$), including the linker region and SANT2 domain, is essential for LSD1-catalyzed demethylation of H3K4 within nucleosomes and that the linker region of CoREST (residues 293−380, abbreviated linker region$^{293-380}$) between the two SANT domains is sufficient to bind LSD1, potentially providing stability to the helical conformation of the LSD1 tower domain (residues 418−522, abbreviated LSD1 tower domain$^{418-522}$) (*4*, *6*, *12*). Consistently, deletional mapping studies (*5*) have shown that the LSD1 tower domain$^{418-522}$ contains the binding site for CoREST.

While many studies have demonstrated the physical interaction between LSD1 and CoREST$^{286-482}$, little is known about the biophysical nature of the interaction and the molecular details of the interaction sites between LSD1 and CoREST. Here, on the basis of the importance of the functional region of CoREST (CoREST$^{286-482}$) in binding to LSD1 as previously studied, we describe the thermodynamic characterization of the binding interaction between LSD1 and CoREST$^{286-482}$ using isothermal titration calorimetry to provide a fundamental understanding of their interaction.

MATERIALS AND METHODS

Reagents and Materials. Media, antibiotics, and all other buffer reagents were purchased from Sigma, New England Biolabs, MP Biomedicals, and BD Biosciences. Chemically competent BL21(DE3) Star *Escherichia coli* cells were purchased from Invitrogen. Chromatographic protein purifications were conducted on an AKTA FPLC system (GE Healthcare), and the protein concentration was determined by UV absorbance spectroscopy. Direct binding studies were performed using isothermal titration calorimetry on a Microcal VP-ITC instrument.

Expression and Purification of LSD1. The gene encoding a truncated form of LSD1 (residues 151−852) (*14*) was used for expression and purification as previously described (*15*, *16*) except that the gene was cloned into the pET15b vector instead of the pET 151-D/TOPO vector for expression. The resulting plasmid was transformed into chemically competent BL21(DE3) Star *E. coli* cells, which were grown on an LB agar plate supplemented with ampicillin overnight at 37 °C. Streaks of the colonies on the plate were used to grow 6 L of cells in TB medium with shaking (200 rpm) at 23 °C. When the cell density reached an OD_{600} of 0.6, 0.5 mM IPTG was added to the flasks to induce LSD1 expression. The cells were allowed to grow overnight and collected by centrifugation at 4225*g*. The cell pellets were lysed with an Emulsiflex C-5 cell cracker in buffer containing 50 mM sodium phosphate, 300 mM NaCl, 5% glycerol, and 0.4 mM PMSF (pH 7.8). LSD1 was then purified by nickel affinity chromatography, HiPrep 26/60 Sephacryl S200 gel filtration chromatography (GE Life Sciences), and anion-exchange chromatography (Q-Sepharose Fast Flow, GE Life Sciences). The final concentration of LSD1 was determined by absorption spectroscopy at 458 nm (*17*), and the protein was stored at −20 °C in 80% glycerol.

Expression and Purification of CoREST$^{286-482}$. A vector encoding a truncated CoREST gene described by Yang et al. (*4*) was constructed and used for expression and purification with the following modifications: the gene was cloned into the pET28b vector, and a gel filtration chromatography step was added for improved purification. The vector was transformed into chemically competent BL21(DE3) Star *E. coli* cells, which were used for purification. Streaks of the colonies on an LB agar containing kanamycin were used to grow 6 L of bacteria. The cells were grown as described above for LSD1 purification. CoREST$^{286-482}$ was purified by nickel affinity chromatography with a linear gradient from 50 to 500 mM imidazole in 50 mM sodium phosphate and 300 mM NaCl (pH 7.4), followed by gel filtration chromatography (HiPrep 26/60 Sephacryl S100, GE Life Sciences) with buffer containing 50 mM sodium phosphate and 100 mM NaCl (pH 7.4), and cation-exchange chromatography (CM-Sepharose Fast Flow, Sigma) with a linear gradient from 100 to 800 mM NaCl in 50 mM sodium phosphate (pH 7.4). The concentration of CoREST$^{286-482}$ was measured spectrophotometrically using an extinction coefficient of 16950 cm^{-1} M^{-1} at 280 nm.

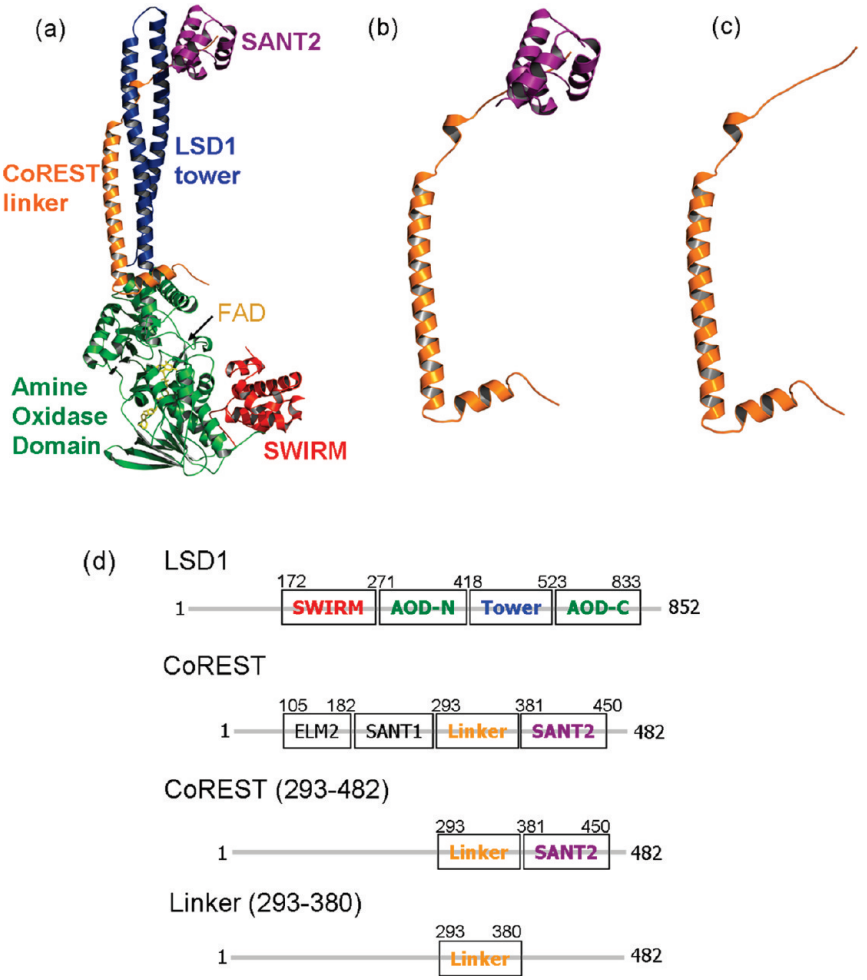

FIGURE 1: Crystal structures of (a) LSD1 in complex with CoREST$^{286-482}$, (b) the functional region of CoREST (CoREST$^{286-482}$) including linker region$^{293-380}$ and SANT2 domain$^{381-450}$, (c) linker region$^{293-380}$ of CoREST, and (d) their domain structures. The three-dimensional structural data file was obtained from Protein Data Bank [entry 2IW5 (*4*)]. The catalytic domain of LSD1, the amine oxidase domain, is colored green; the SWIRM domain of LSD1 red; and the tower region of LSD1 blue. FAD is denoted by a black arrow and is colored yellow. SANT2 domain$^{381-450}$ of CoREST is colored purple, and linker region$^{293-380}$ of CoREST is colored orange. All structural figures were generated using PyMoL.

Expression and Purification of Linker Region$^{293-380}$ and SANT2 Domain$^{381-450}$ of CoREST. The coding sequence of the linker region (resisdues 293−380) of CoREST was extracted and amplified by using PCR with a forward primer (5′-GCGCATATGGTCAAAAAAGAAAAACATAGCACACAAGCTAAA-3′) and a reverse primer (5′-GCGCTCGAGTTAATTACATTTCTGAATGACCTCTGGAGG-3′) under the following conditions: an initial denaturation step for 5 min at 95 °C, 30 cycles of denaturation for 1 min at 95 °C, annealing for 1 min over a gradient from 54 to 65 °C, elongation for 100 s at 70 °C, and a final elongation step for 10 min at 70 °C. The primers were designed to contain NdeI and XhoI restriction sites at the N- and C-termini, respectively, to allow for facile ligation into the pET28b vector. The vector was transformed into chemically competent BL21(DE3) Star *E. coli* cells, and the cells were grown overnight as described above for LSD1 purification. The cell pellets were lysed with an Emulsiflex C-5 cell cracker in buffer containing 50 mM sodium phosphate, 300 mM NaCl, 5% glycerol, and 0.4 mM PMSF (pH 7.8). The linker region was then purified via nickel-affinity chromatography with a linear gradient from 50 to 500 mM imidazole in 50 mM sodium phosphate and 300 mM NaCl (pH 7.8), followed by cation-exchange chromatography (SP-Sepharose Fast Flow, Sigma) with a linear gradient from 100 to 800 mM NaCl in 50 mM sodium phosphate (pH 7.8). The protein concentration was measured spectrophotometrically at 280 nm with an extinction coefficient of 1490 cm^{-1} M^{-1}.

The gene encoding the SANT2 domain$^{381-450}$ of CoREST was extracted, amplified by PCR with a forward primer (5′-GCGCATATGGCACGTTGGACTACAGAAGAGCAGCTT-3′) and a reverse primer (5′-GCTCTCGAGTTAACTGGGCCCATTGGTCTCTTCTTTACC-3′), and ligated into the pET 28b vector. The vector was transformed into chemically competent BL21-(DE3) Star *E. coli* cells, and cells were grown overnight as described above for LSD1 purification. The SANT2 domain was purified via nickel-affinity chromatography with a linear gradient from 50 to 500 mM imidazole in 50 mM MES and 300 mM NaCl (pH 6.0) and cation-exchange chromatography (SP-Sepharose Fast Flow, Sigma) with a gradient from 100 to 800 mM NaCl in 50 mM MES (pH 6.0). The protein concentration was measured spectrophotometrically at 280 nm using an extinction coefficient of 13980 cm^{-1} M^{-1}.

Enzymatic Assay. Steady-state kinetic assays for determining kinetic parameters for LSD1 activity on the dimethylated H3K4 21-mer peptide substrate with and without CoREST$^{286-482}$ were performed by employing a fluorescence assay as previously described (*15*, *16*). All assays were performed at 25 °C, and the product was monitored with a fluorescence plate reader

(Molecular Devices SpectraMax Germini EM) with 560 nm excitation and 590 nm emission wavelengths. The experiment was performed in duplicate.

Isothermal Titration Calorimetry (ITC). ITC experiments were performed using a MicroCal VP-ITC microcalorimeter (MicroCal, Northampton, MA) with a cell volume of 1.4346 mL. Protein samples were dialyzed against the buffer containing 50 mM sodium phosphate and 1 mM DTT (pH 7.4) and vacuum-degassed for at least 30 min before being loaded into the calorimeter. Approximately 1.5 mL of the degassed LSD1 and buffer were placed in the sample cell and reference cell, respectively, and CoREST$^{286-482}$ was loaded into the syringe injector. In most ITC experiments, 3 μL aliquots of CoREST$^{286-482}$ at a concentration of 30 μM were titrated sequentially against LSD1 at a concentration of 3 μM in the sample cell at 25 °C. Each injection lasted for 6 s, and there was a delay of 300 s between injections. During the titration, the stirring speed was 310 rpm and a total of 40−60 injections of CoREST$^{286-482}$ were titrated into LSD1. A one-site binding model (Origin version 5.0, MicroCal Software, Inc.) was used to fit the data. The titrations were performed under different experimental conditions such as various buffers, a temperature range of 15−35 °C, different pHs, and changes of buffer additives. For titrations of linker region$^{293-380}$ or SANT2 domain$^{381-450}$ of CoREST against LSD1, 3 μL aliquots of linker region$^{293-380}$ or SANT2 domain$^{381-450}$ at a concentration of 30 μM were titrated sequentially into 1.5 mL of LSD1 at a concentration of 3 μM at 25 °C under the same experimental conditions described above for the titration of CoREST$^{286-482}$ against LSD1.

Surface Plasmon Resonance (SPR) Measurements. All SPR measurements were made using a BIAcore 3000 instrument, and data analyses were performed using BIAevaluation version 4.1 (BIAcore). CoREST$^{286-482}$ was immobilized [~2200 response units (RU)] on a BIAcore CM5 (research grade) chip using standard amine coupling chemistry with reagents obtained from BIAcore. In a parallel flow cell, LSD1 was immobilized (~2500 RU). During the screening experiments with 50 mM sodium phosphate and 1 mM DTT (pH 7.4) as a running buffer, LSD1 was injected over immobilized CoREST$^{286-482}$ for 2 min at a flow rate of 30 μL/min to monitor the binding interaction. The surfaces were regenerated via injection of 10 μL of glycine (pH 2.0) at a flow rate of 50 μL/min. The response from the LSD1 surface was used to subtract out the background (nonspecific) signal. The K_d value of the LSD1−CoREST$^{286-482}$ interaction was estimated via injection of LSD1 in buffer containing 50 mM sodium phosphate and 1 mM DTT (pH 7.4) for 3 min at various concentrations ranging from 6.25 to 62.5 nM. A global fitting of binding curves at different concentrations with the Langmuir binding model was used to measure the association (k_{on}) and dissociation (k_{off}) rates and the apparent affinity constant (K_a).

Calculation of the Solvent Accessible Surface Area (ASA). The solvent accessible surface area (ASA) of the LSD1−CoREST$^{286-482}$ complex was estimated with three different programs, GetArea (*18*), PIBASE (*19*), and PISA (*20*), with the radius of the probe set to 1.4 Å. The structural data file of LSD1 in complex with CoREST$^{286-482}$ (*4*) was obtained from the Protein Data Bank (entry 2IW5) and used to calculate the parameters.

RESULTS

Expression and Purification of LSD1 and CoREST$^{286-486}$. A recombinant protein variant of human LSD1 with a deletion of the first 150 amino acids at the N-terminus was expressed and purified as previously described (*14*−*16*). Purified LSD1 was visualized on a 15% SDS−PAGE gel by Coomassie Blue staining (Figure 2a). A His$_6$-tagged CoREST$^{286-482}$, including the linker region and SANT2 domain, was expressed in several *E. coli* strains under different growth conditions to determine the optimal yield. BL21(DE3) Star *E. coli* cells exhibited the best expression of CoREST$^{286-482}$. Although a higher temperature (37 °C) led to increased expression, the cells were grown at a lower temperature (23 °C) to yield soluble protein. Purified CoREST$^{286-482}$ was run on a 15% SDS−PAGE gel (Figure 2b). To define the crucial role of linker region$^{293-380}$ of CoREST in binding to LSD1, linker region$^{293-380}$ and SANT2 domain$^{381-450}$ of CoREST were individually expressed and purified from BL21(DE3) Star *E. coli*. They were run on 4 to 20% gradient SDS−PAGE gels (Figure 2c for linker region$^{293-380}$ and Figure 2d for SANT2 domain$^{381-450}$ of CoREST).

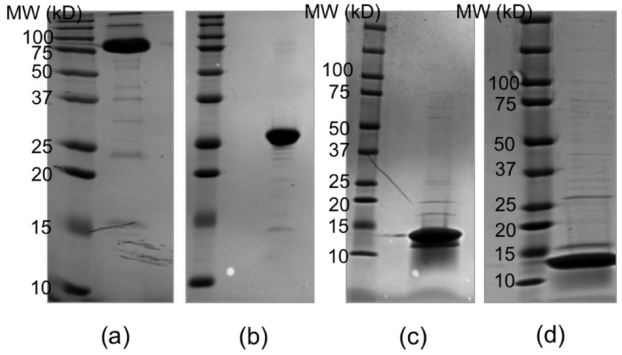

FIGURE 2: Fifteen percent SDS−PAGE gels of (a) purified LSD1 and (b) purified CoREST$^{286-482}$. Four to twenty percent gradient SDS−PAGE gels of (c) linker region$^{293-380}$ and (d) SANT2 domain$^{381-450}$ of CoREST. Kaleidoscope prestained standards were used (Bio-Rad).

Table 1: Kinetic Parameters of the Catalytic Activity of LSD1 with the First 21 Amino Acids of H3 with Dimethylated K4[a]

	initial velocity (μM/s)	K_M (μM)	k_{cat} (s^{-1})
LSD1 only	0.028 ± 0.002	2.300 ± 0.305	0.057 ± 0.003
LSD1−CoREST$^{286-482}$	0.046 ± 0.001	8.833 ± 1.559	0.092 ± 0.001

[a]In 50 mM Tris buffer (pH 7.85) at 25 °C; 19.9 mM peptide substrate used.

Enzymatic Assays. The demethylation activity of LSD1 against several methylated peptides of varying lengths has been previously reported (*17*, *21*), showing that the first 21 amino acids of H3, including dimethylated K4, were sufficient for detectable LSD1 activity. As such, we evaluated kinetic parameters for LSD1 activity on a peptide consisting of the first 21 N-terminal amino acids of H3 with dimethylated K4 by using GraFit version 6.0 (Erithacus Software, West Sussex, U.K.); kinetic parameters and representative data are listed and shown in Table 1 and Figure 3, respectively. Derived kinetic values are in reasonable agreement with previously reported values (*17*, *21*). The incubation of LSD1 with CoREST$^{286-482}$ for 2 h at 4 °C increased the initial velocity of the catalytic activity of LSD1 roughly 1.6-fold and decreased the catalytic efficiency (k_{cat}/K_M). Thus, CoREST$^{286-482}$ has little impact on the catalytic efficiency of LSD1 toward peptide substrates. However, it is possible that the catalytic efficiency may be increased when nucleosomal substrates are used because CoREST$^{286-482}$ is known to stimulate the catalytic activity of LSD1 toward nucleosomal substrates.

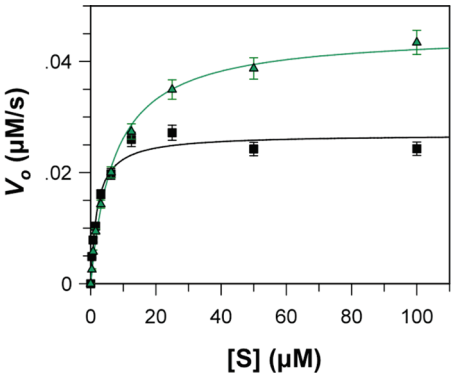

FIGURE 3: Initial velocity curves of the catalytic activity of LSD1 using the first 21 amino acid residues of H3 with dimethylated K4 as a substrate. The assay was performed in 50 mM Tris buffer (pH 7.85) at 25 °C, and the final concentration of both proteins was 0.5 μM. Data were fitted to the Michaelis−Menten equation. The black curve represents the activity of LSD1, whereas the green curve represents the activity of LSD1 incubated with CoREST$^{286-482}$.

Calorimetric Titration of CoREST$^{286-482}$ against LSD1. Previous studies have demonstrated an interaction between CoREST$^{286-482}$ and LSD1 (*4*, *5*), but little biophysical information about the interaction exists. Initial experiments for studying this binding interaction were performed using a MicroCal VP-ITC microcalorimeter at 25 °C. Calorimetric data were analyzed using Origin version 5.0. To correct data for dilution, average heats observed in the last 10−15 injections were subtracted from binding data. The data were then fit to a one-site binding model to give the stoichiometry (n), association constant (K_a), and change in binding enthalpy (ΔH). The free energy of association (ΔG) and change in entropy ($T\Delta S$) were calculated from the known thermodynamic relationships.

ITC experiments with LSD1 and CoREST$^{286-482}$ yielded the thermogram shown in Figure 4a, displaying raw power output versus time of CoREST$^{286-482}$ injection into the cell containing LSD1 (top panel) and the corresponding binding where the enthalpy per mole of CoREST$^{286-482}$ as a function of LSD1 is plotted (bottom panel). Each injection of CoREST$^{286-482}$ gave rise to exothermic heats of binding, and each peak became smaller as the binding sites on LSD1 were saturated with CoREST$^{286-482}$. Thermodynamic parameters for the interaction are summarized in Table 2. The dissociation constant (K_d) for LSD1−CoREST$^{286-482}$ interaction was determined to be 15.9 ± 2.07 nM, indicating a tight binding between LSD1 and CoREST$^{286-482}$. The thermodynamic parameters of binding of LSD1 to CoREST$^{286-482}$ showed overall favorable enthalpic (−21.3 ± 0.19 kcal/mol) and unfavorable entropic (−10.7 ± 1.40 kcal/mol) contributions near room temperature. The stoichiometry is close to 1, suggesting a simple 1:1 complex.

Surface Plasmon Resonance (SPR) Measurements. The tight binding interaction between LSD1 and CoREST$^{286-482}$ was confirmed by surface plasmon resonance measurements. As shown in Figure 4b, the increase in response units over time represents the amount of LSD1 bound to CoREST$^{286-482}$ that is proportional to the association rate constant (k_{on}, $5.63 \times 10^4 \pm 1.93 \times 10^3$ M^{-1} s^{-1}) of the binding interaction. After association, buffer was injected to dissociate the bound LSD1, which results in the decrease in response units over time and yields a dissociation rate constant (k_{off}, $7.78 \times 10^{-5} \pm 1.27 \times 10^{-5}$ s^{-1}). Some noises observed in the dissociation phase after 300 s, which might affect uncertainty in the determination of the dissociation rate constant

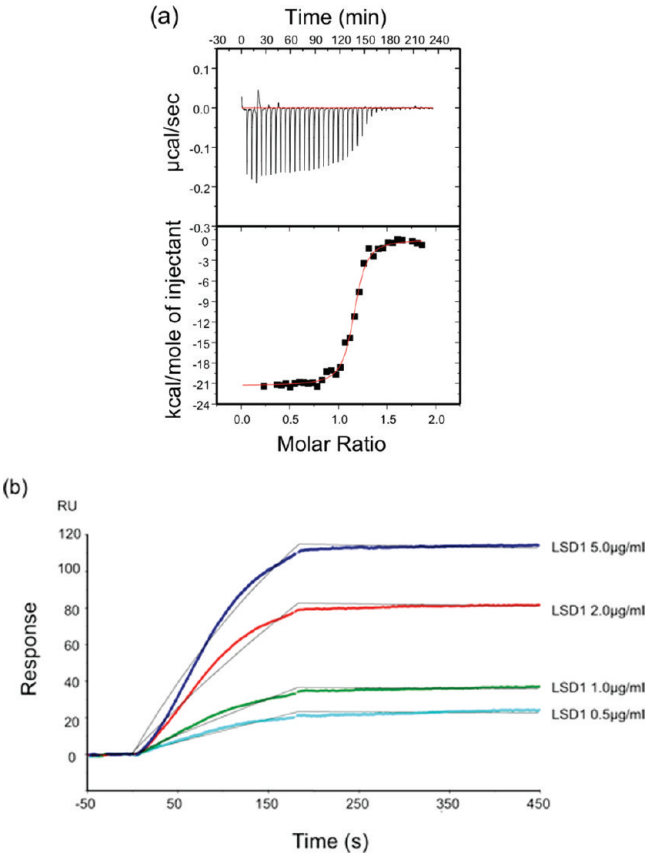

FIGURE 4: (a) Representative calorimetric titration of 3 μM LSD1 with 30 μM CoREST$^{286-482}$ in 50 mM sodium phosphate and 1 mM DTT (pH 7.4). The thermogram (top) represents the heat released after each injection of CoREST$^{286-482}$ into the LSD1 solution. The binding isotherm (bottom) shows the integrated peak area plotted as a function of molar ratio (CoREST$^{286-482}$: LSD1). The following parameters were observed: $n = 1.14 \pm 0.00$, $\Delta H = -21.3 \pm 0.19$ kcal/mol, and $K_a = 6.29 \times 10^7 \pm 8.18 \times 10^6$ M^{-1}. The red line indicates the best fit of the ITC data to a one-site binding model. (b) Surface plasmon resonance measurement curves obtained during and after injection of LSD1 onto chip surfaces with immobilized CoREST$^{286-482}$. Sensorgrams show the association of LSD1 to and dissociation from CoREST$^{286-482}$.

(k_{off}), were removed. These rate constant values suggest a dissociation constant (K_d) of 1.4 ± 6.61 nM, slightly lower than the dissociation constant (15.9 ± 2.07 nM) measured using isothermal titration calorimetry. The small but significant differences between binding constants obtained from two techniques reflect a small degree of enhanced binding during SPR measurement. This difference in binding constants may also be attributed to a slow off rate caused by a columning phenomenon frequently observed in SPR experiments (*22*). Nonetheless, these techniques independently confirm that the interaction between LSD1 and CoREST$^{286-482}$ is tight and specific and proceeds with a 1:1 stoichiometry.

Calorimetric Titrations of CoREST$^{286-482}$ against LSD1 in Different Buffers. The observed calorimetric enthalpy may not solely arise from the binding interaction, because several other events contribute to the heats of binding (*23*−*25*). One such event is the transfer of a proton between a protein−protein complex and buffer because of the shift in protein pK_a on complex formation and buffer ionization. Such proton transfer can be parsed by the following expression:

$$\Delta H_{cal} = \Delta H_{intrinsic} + N\Delta H_{ion}$$

Table 2: Thermodynamic Parameters for Binding of LSD1 to CoREST$^{286-482}$ and Linker Region$^{293-380}$ of CoREST[a]

	K_d (nM)	ΔH (kcal/mol)	$T\Delta S$ (kcal/mol)	ΔG (kcal/mol)	stoichiometry
LSD1−CoREST$^{286-482}$	15.9 ± 2.07	−21.3 ± 0.19	−10.7 ± 1.40	−10.6 ± 1.38	1.14 ± 0.00
LSD1−CoREST$^{293-380}$	7.78 ± 3.50	−13.5 ± 0.37	−2.42 ± 1.09	−11.1 ± 5.00	0.96 ± 0.01

[a]In 50 mM sodium phosphate and 1 mM DTT (pH 7.4).

Table 3: Thermodynamic Parameters for Binding of LSD1 to CoREST$^{286-482}$ in Various Buffers at 25 °C[a]

buffer	K_d (nM)	ΔH_{cal} (kcal/mol)	$T\Delta S$ (kcal/mol)	ΔG (kcal/mol)	stoichiometry
phosphate	17.3 ± 3.98	−19.5 ± 0.26	−8.93 ± 2.06	−10.6 ± 2.44	1.11 ± 0.01
PIPES	5.84 ± 1.63	−17.4 ± 0.32	−6.19 ± 1.75	−11.2 ± 3.17	0.91 ± 0.01
HEPES	11.7 ± 4.20	−15.2 ± 0.38	−4.33 ± 1.57	−10.9 ± 3.93	1.01 ± 0.01
ACES	21.2 ± 7.82	−12.6 ± 0.41	−2.48 ± 0.93	−10.1 ± 3.77	0.93 ± 0.02
Tris	8.54 ± 3.50	−10.9 ± 0.28	−0.12 ± 0.05	−10.8 ± 4.45	0.92 ± 0.01

[a]In 50 mM sodium phosphate (PIPES, HEPES, ACES, and Tris) and 1 mM DTT (pH 7.4).

where ΔH_{cal} is the sum of calorimetric enthalpy, $\Delta H_{intrinsic}$ is the enthalpy of binding in the absence of protonation effects, N is the number of protons transferred during binding, and ΔH_{ion} is the enthalpy of buffer ionization. A negative slope of the plot of ΔH_{cal} versus ΔH_{ion} indicates a net release of protons from protein to the buffer, while a positive slope indicates a net uptake of protons by the protein from the buffer (*23*). To assess the contribution of the heat of ionization upon binding, we performed titrations in five buffers with different heats of ionization: sodium phosphate (ΔH_{ion} = 0.9 kcal/mol), PIPES (ΔH_{ion} = 2.7 kcal/mol), HEPES (ΔH_{ion} = 5.7 kcal/mol), ACES (ΔH_{ion} = 7.5 kcal/mol), and Tris (ΔH_{ion} = 11.4 kcal/mol) (*26*). Table 3 shows thermodynamic parameters for the binding between LSD1 and CoREST$^{286-482}$ in various buffers at pH 7.4. A plot of ΔH_{cal} versus ΔH_{ion} (Figure 5a) yielded a straight line with a positive slope, indicating that 0.83 ± 0.09 proton is absorbed by the LSD1−CoREST$^{286-482}$ complex from the buffer at pH 7.4. $\Delta H_{intrinsic}$ (i.e., when ΔH_{ion} = 0) was determined to be −19.8 ± 0.58 kcal/mol, suggesting that the binding interaction is intrinsically exothermic and enthalpy-driven at room temperature.

Calorimetric Titrations of CoREST$^{286-482}$ against LSD1 at Different Temperatures. In addition to the contribution of a proton transfer to the binding interaction, another important contribution to binding enthalpy comes from solvent reorganization upon binding (*23*). The thermodynamic parameter most closely associated with solvent reorganization is the change in constant-pressure heat capacity (ΔC_p). The change in heat capacity (ΔC_p) was obtained by measuring ΔH over the temperature range of 15−35 °C in 50 mM sodium phosphate buffer with 1 mM DTT (pH 7.4) (Table 4). At a low temperature (10 °C), the signals generated upon binding were too small to fit to a binding model. Titrations at a high temperature (55 °C) yielded an irregular binding curve, suggesting protein denaturation.

A plot of ΔH versus temperature yielded a straight line with a negative slope (ΔC_p), −0.80 ± 0.01 kcal mol^{-1} K^{-1} (Figure 5b). The major contributions to ΔC_p originate from hydrophobic, conformational, and vibrational effects (*27*), but hydrophobic interactions are dominant contributors (*28*, *29*). The crystal structure of the LSD1−CoREST$^{286-482}$ complex shows that the binding interface between LSD1 and CoREST$^{286-482}$ is mostly populated by nonpolar residues that are presumably involved in hydrophobic interactions during formation of the complex (Figure 6b). Also, the effect of NaCl on the change in heat capacity (ΔC_p) was studied over the same temperature range, using

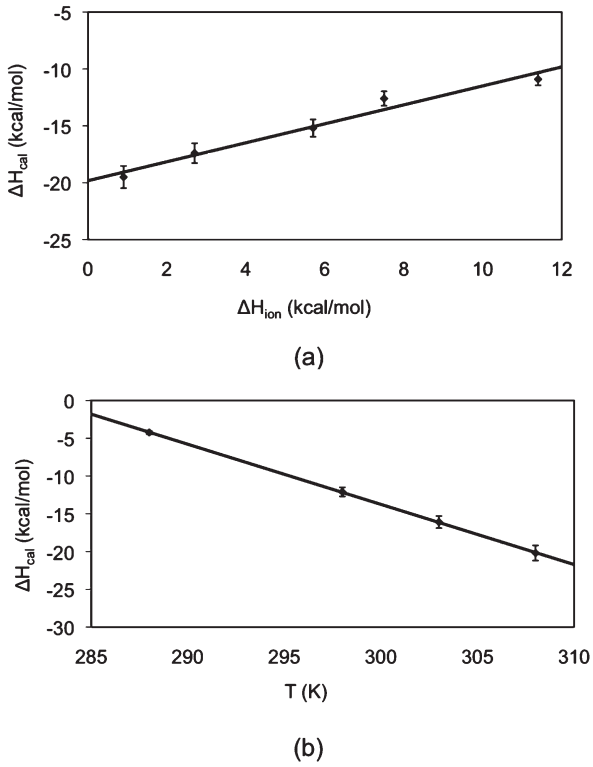

FIGURE 5: (a) Plot of the calorimetric enthalpy (ΔH_{cal}) obtained from binding of LSD1 to CoREST$^{286-482}$ as a function of the buffer ionization enthalpy (ΔH_{ion}) at pH 7.4. The slope of the plot indicates the number of protons transferred between the complex and the buffer upon binding, and the *y*-intercept indicates the intrinsic ΔH without a protonation effect. At pH 7.4, 0.83 ± 0.09 proton is absorbed to the complex from the buffer. (b) Temperature dependence of the binding enthalpy change for the interaction between LSD1 and CoREST$^{286-482}$. The slope of the plot yields the binding heat capacity change (ΔC_p), which is equal to −0.80 ± 0.01 kcal mol^{-1} K^{-1}.

varying concentrations of NaCl (10 and 100 mM) in 50 mM sodium phosphate buffer with 1 mM DTT (pH 7.4). As the concentration of NaCl in buffer increased, larger binding heats (ΔH) were observed, but ΔC_p values did not vary significantly. The ΔC_p values with the addition of 10 and 100 mM NaCl were determined to be −1.04 ± 0.04 and −0.84 ± 0.1 kcal mol^{-1} K^{-1}, respectively.

Calculation of the Solvent Accessible Surface Area. The solvent accessible surface area (ASA) has been used to predict

Table 4: Thermodynamic Parameters for Binding of LSD1 to CoREST$^{286-482}$ at Different Temperatures[a]

T (°C)	K_d (nM)	ΔH (kcal/mol)	$T\Delta S$ (kcal/mol)	ΔG (kcal/mol)	stoichiometry
15	21.7 ± 10.9	−4.24 ± 0.17	5.86 ± 2.95	−10.1 ± 5.07	0.99 ± 0.02
25	3.18 ± 2.54	−12.1 ± 0.39	−0.49 ± 0.39	−11.6 ± 9.27	1.01 ± 0.02
30	3.70 ± 1.74	−16.1 ± 0.27	−4.42 ± 2.08	−11.7 ± 5.50	1.03 ± 0.01
35	8.03 ± 4.10	−20.2 ± 0.57	−8.79 ± 4.49	−11.4 ± 5.82	0.97 ± 0.02

[a]In 50 mM sodium phosphate and 1 mM DTT (pH 7.4).

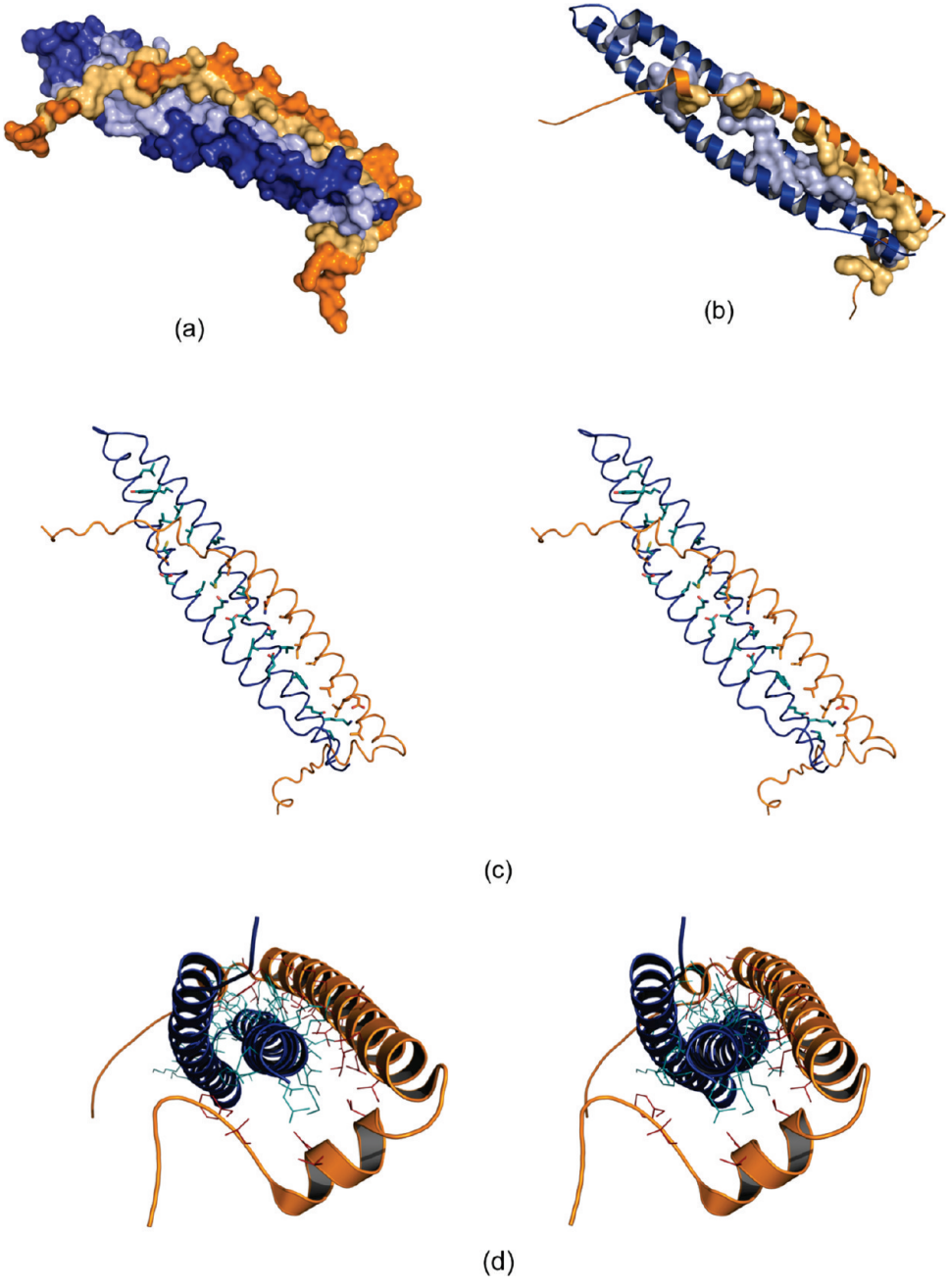

FIGURE 6: (a) Surface representation of the binding interface between LSD1 tower region$^{418-522}$ and linker region$^{293-380}$ of CoREST. The blue and orange surfaces represent LSD1 tower domain$^{418-522}$ and linker region$^{293-380}$ of CoREST, respectively. On the basis of information from the three-dimensional structure of the complex, pale blue and orange surfaces indicate the surface of each protein involved in key binding interactions. (b) Nonpolar residues at the binding interface. LSD1 tower domain$^{418-522}$ and linker region$^{293-380}$ of CoREST are represented in a ribbon diagram, and nonpolar residues involved in the binding interface are represented by a surface diagram. (c) Stereoview of packing in the trimeric coiled-coil interaction between LSD1 tower region$^{418-522}$ (blue) and linker region$^{293-380}$ (orange) of CoREST. The side chains at positions a and d of a heptad repeat model are represented as sticks. (d) Stereoview (from the top) of the binding interface. All residues involved in the binding interaction are represented by lines.

structural information about proteins (*29*, *30*). The ASA of the binding interface calculated by three different programs was predicted to be ~2500 Å, and the ASA buried at the interface was determined to be approximately 5498.0 Å, with a polar:nonpolar

Table 5: Thermodynamic Parameters for Binding of LSD1 to CoREST$^{286-482}$ at Different pHs (25 °C)[a]

pH	K_d (nM)	ΔH (kcal/mol)	$T\Delta S$ (kcal/mol)	ΔG (kcal/mol)	stoichiometry
6.0	4.18 ± 0.96	−8.56 ± 0.01	2.87 ± 0.66	−11.4 ± 2.62	0.90 ± 0.004
7.0	6.75 ± 1.49	−12.9 ± 0.15	−1.54 ± 0.34	−11.4 ± 2.51	1.00 ± 0.01
8.0	7.66 ± 2.91	−15.6 ± 0.32	−4.48 ± 1.71	−11.1 ± 4.22	1.00 ± 0.01
9.0	nb[b]	nb[b]	nb[b]	nb[b]	nb[b]

[a]In 50 mM sodium phosphate, 50 mM glycine, and 1 mM DTT (pH 6.0); 50 mM sodium phosphate, 50 mM glycine, and 1 mM DTT (pH 7.0); 40 mM sodium phosphate, 30 mM glycine, and 1 mM DTT (pH 8.0); and 40 mM sodium phosphate, 30 mM glycine, and 1 mM DTT (pH 9.0). [b]No binding (nb) curve observed.

ratio ($ASA_{polar\ buried}/ASA_{nonpolar\ buried}$ = 1695.2 Å/3802.8 Å) of 0.446. The amount of buried nonpolar surface area estimated was 70% of the interfacial surface, which was presumably the main contributor to the observed negative ΔC_p.

Calorimetric Titrations of CoREST$^{286-482}$ against LSD1 as a Function of pH. The effect of pH on the thermodynamic parameters of the binding interaction was studied over the pH range of 6.0−9.0 in a buffer system with a constant ionic strength. At pH 6.0 and 7.0, the buffer consisted of 50 mM sodium phosphate, 50 mM glycine, and 1 mM DTT, whereas 40 mM sodium phosphate, 30 mM glycine, and 1 mM DTT were used for experiments at pH 8.0 and 9.0. The pH range was selected on the basis of previous reports of the stability and activity of LSD1 (*16*, *17*). Table 5 demonstrates that while a change in pH produces no significant change in affinity, there is a trend toward a more favorable enthalpic contribution and a larger entropic penalty as pH increases. These changes in enthalpic and entropic contributions to free energy as the pH increases can be rationalized by changes in the protonation state of residues that may cause slight perturbations from the optimal binding interaction between LSD1 and CoREST$^{286-482}$. At pH 9.0, a binding isotherm was not observed. High pH presumably alters the structure of LSD1, CoREST$^{286-482}$, or both, changing their binding interaction. Previous work has shown that the catalytic activity of LSD1 is diminished at pH > 9.5 (*16*), in accord with our observations at pH 9.0.

Effect of Disulfide Bond Formation on the Binding Interaction. A cysteine from LSD1 tower domain$^{418-522}$ (residue 491) and another from CoREST$^{286-482}$ (residue 379) are present at the binding interface: these residues can presumably participate in disulfide bonds. Concomitant protein oxidation leading to the mixed disulfide bonds between LSD1 and CoREST$^{286-482}$ would confound interpretation of thermodynamic data. To study the effect of disulfide bond formation upon binding, titrations were performed at 25 °C (pH 7.4) with buffer containing only 50 mM sodium phosphate without DTT. The thermodynamic parameters measured under these conditions were in reasonable agreement with those obtained with the buffer containing 1 mM DTT. On the basis of these data, we concluded that derived thermodynamic parameters do not include contributions from disulfide bond formation.

Calorimetric Titration of CoREST Linker Region$^{293-380}$ and SANT2 Domain$^{381-450}$ against LSD1. Titrations of linker region$^{293-380}$ against LSD1 were performed at 25 °C (pH 7.4) to define the role of linker region$^{293-380}$ in complex formation and to study thermodynamic parameters for the binding interaction with LSD1. Table 2 shows that although smaller enthalpic and entropic changes were observed in the binding interaction between LSD1 and linker region$^{293-380}$ compared to the those for binding between LSD1 and CoREST$^{286-482}$, there is no significant difference in affinity, with a K_d of 7.78 ± 3.50 nM. Interestingly, the titration of the SANT2 domain$^{381-450}$ of CoREST against LSD1 showed no binding (Figure 1S of the Supporting Information) under the same experimental condition, indicating no or only very weak binding. This result indicates that the residues crucial for the interaction with LSD1 lie in linker region$^{293-380}$, and the lack of the binding interaction observed between LSD1 and SANT2 domain$^{381-450}$ supports the importance of linker region$^{293-380}$ for LSD1 binding.

DISCUSSION

In this study, thermodynamic parameters for the binding interaction between LSD1 and CoREST$^{286-482}$ were determined calorimetrically. ITC experiments demonstrate that the binding between LSD1 and CoREST$^{286-482}$ is a tight interaction with a dissociation constant (K_d) in the nanomolar range, and that important residues involved in the binding interaction are localized within linker region$^{293-380}$. The high binding affinity is attributed to various noncovalent interactions between LSD1 and CoREST$^{286-482}$ upon binding as shown in Figure 6. In addition to the helical interactions between linker region$^{293-380}$ and LSD1 tower domain$^{418-522}$, the N-terminal region of CoREST$^{286-482}$ wraps around the bottom of the antiparallel helices of LSD1 tower domain$^{418-522}$, contributing to the overall strength of the binding.

Most thermodynamic data for the binding between LSD1 and CoREST$^{286-482}$ showed enthalpies of interaction greater than the free energies of association and unfavorable entropies of association, which is commonly observed in biomolecular interactions. In the binding interaction between LSD1 and CoREST$^{286-482}$, the favorable change in enthalpy reflects a net increase in the number or strength of bonds formed between two proteins. On the basis of the known crystal structure of the LSD1−CoREST$^{286-482}$ complex (*4*, *5*), several candidates for the formation of hydrogen bonds and salt bridges at the interface are found; interactions between residues F315, D320, D339, K353, N356, K360, and R371 of linker region$^{293-380}$ of CoREST and Q419, K421, K424, Q438, D495, E505, and E512 of LSD1 tower domain$^{418-522}$ may contribute directly to the enthalpic gain. The entropy of association can be affected by contributions associated with proteins and solvent (*31*). The unfavorable entropies of binding observed most likely can be ascribed to the contributions from conformational changes upon binding. Previous studies showed a linear correlation of the change in the conformational entropy with the change in the total entropy of binding (*31*).

Conformational changes occurring in the binding interaction between LSD1 and CoREST$^{286-482}$ can affect the environment of amino acid residues and thus their pK_a values (*23*). This results in the transfer of protons between the buffer and ionizable groups of amino acid residues. As this process contributes to the sum of the calorimetric enthalpy change, measured changes must be corrected for the proton transfer effects. To perform this correction, we analyzed the formation of the LSD1−CoREST$^{286-482}$ complex in buffers with different ionization enthalpies. The positive slope (0.83 ± 0.09) of the plot of ΔH_{cal} versus ΔH_{ion}

demonstrates that the LSD1−CoREST$^{286-482}$ complex takes up approximately one proton from the buffer system at pH 7.4. Presumably, this protonation event involves either lysine or arginine in the LSD1−CoREST$^{286-482}$ complex near neutral pH.

It is widely known that protein−protein interaction is driven by hydrophobic interactions to a large extent, which results in a negative change in heat capacity (*28*, *29*). The change in heat capacity of the binding interaction between LSD1 and CoREST$^{286-482}$ obtained from the slope of the linear temperature dependency of the change in enthalpy was negative as predicted on the basis of the structural features of the complex (Figure 6b). In addition, the change in accessible surface area (ΔASA) allows us to calculate the empirical heat capacity change by the following equation (*32*):

$$\Delta C_p = 0.36 \text{ cal mol}^{-1} \text{ K}^{-1} \text{ Å}^{-2} (\Delta\text{ASA}_{\text{nonpolar}}) - 0.25 \text{ cal mol}^{-1} \text{ K}^{-1} \text{ Å}^{-2} (\Delta\text{ASA}_{\text{polar}})$$

where $\Delta\text{ASA}_{\text{nonpolar}}$ is the change in nonpolar accessible surface area, $\Delta\text{ASA}_{\text{polar}}$ is the change in polar accessible surface area, and 0.36 and −0.25 are empirical constants for the nonpolar and polar surface area, respectively. The calculation of $\Delta\text{ASA}_{\text{nonpolar}}$ and $\Delta\text{ASA}_{\text{polar}}$ was performed using GetArea (*18*). The values of the changes in polar, nonpolar, and total accessible surface area are summarized in Table 1S of the Supporting Information. The value of the change in heat capacity predicted by the equation above is −1.16 kcal mol^{-1} K^{-1}, which is somewhat larger than the experimentally determined value of −0.80 kcal mol^{-1} K^{-1}, but which is in at least qualitative agreement. This result allows us to conclude that the nonpolar surface area contributes more to the buried surface, in agreement with the negative change in heat capacity.

Our thermodynamic parameters for the interaction between LSD1 and CoREST$^{286-482}$ can be rationalized in terms of the structure of the binding interface. Linker region$^{293-380}$ of CoREST is clearly important for binding to LSD1, with thermodynamic parameters in reasonable accordance with those for the binding between LSD1 and CoREST$^{286-482}$. In contrast, no binding isotherm was observed during titration between LSD1 and SANT domain$^{381-450}$. LSD1 tower domain$^{418-522}$ was previously reported to be sufficient for interaction with CoREST (*5*). These data led us to conclude that the binding interface occurs between LSD1 tower domain$^{418-522}$ and linker region$^{293-380}$, and for this reason, only linker region$^{293-380}$ and LSD1 tower domain$^{418-522}$ are considered for our detailed interaction study.

As shown in Figure 6c and 6d, the binding interface consists of three α-helices: one helix from linker region$^{293-380}$ (orange-colored) and two antiparellel helices from LSD1 tower domain$^{418-522}$ (blue-colored). This type of interaction is typically classified as a coiled-coil interaction and is found in various proteins, including intermediate filaments, cell surface receptors, molecular motors, and transcription factors (*33*). Like the interaction between LSD1 tower domain$^{418-522}$ and linker region$^{293-380}$, trimeric coiled-coil interactions have been reported in various studies of the oligomerization domains of hemagglutinin membrane glycoprotein (*34*), C-type mannose-binding protein (*35*), mechanisms of laminin chain assembly (*36*), the crystal structure of GCN4-pI_{Q}I (*37*), and the crystal structure of de novo-designed $\text{V}_{\text{a}}\text{L}_{\text{d}}$ (*38*).

Coiled-coil interactions are usually characterized by a heptad repeat sequence $(\text{abcdefg})_n$ (*39*−*42*), with hydrophobic residues at positions a and d whose interaction is well-known as a main driving force for the stability of helical conformations, and polar or charged residues at positions e and g, providing further stability to the coiled-coil interaction through ionic interactions. However, unlike this classic periodicity, all the hydrophobic residues of three α-helices in the LSD1−CoREST$^{286-482}$ complex are not assigned at positions a and d. The presence of polar residues such as asparagine, glutamine, glutamic acid, and lysine is observed at those positions, suggesting their role in the formation of hydrogen bonds and ionic interactions. This structural feature presumably compensates for the destabilizing effect of desolvation (*43*, *44*).

For a more detailed analysis at a molecular level, the binding interface was dissected into three portions. The first consists of two α-helices of an N-terminus of the linker region$^{293-380}$ of CoREST and an N-terminus of LSD1 tower domain$^{418-522}$, and a tail of a C-terminus of LSD1 tower domain$^{418-522}$ (Figure 7a). Most of the interactions in the first region of the interface originate from hydrophobic contacts, with two hydrogen bonds formed between D339 of CoREST and K424 of LSD1 and between D320 of CoREST and K421 of LSD1. The second region of the interface consists of three α-helices, which comprise residues 433−450 and 496−513 of LSD1 and residues 345−365 of CoREST. Several hydrogen bonds and ionic interactions are observed at this interface, as well as hydrophobic packing (Figure 7b). Interestingly, three residues (K353, N356, and K360) in linker region$^{293-380}$, which occupy periodically almost equivalent positions, are involved in both hydrogen bonds and salt bridge formation with both α-helices of LSD1 tower domain$^{418-522}$ contributing to the tight binding interaction. The third region of the interface, defined by residues 451−495 of LSD1 and residues 366−380 of CoREST, includes antiparallel α-helices of LSD1 tower domain$^{418-522}$ with a loop and a single turn of α-helix of linker region$^{293-380}$ with R371 at the end of the helix (Figure 7c). R371 of CoREST interacts with D495 on one helix of LSD1 at a distance of ∼2.6 Å. On the basis of this structural study, the important binding interactions seem to be localized to the second region of the interface where all three helices are held tightly by several noncovalent interactions. However, the first and third regions of the interface also play an important role in the overall binding interaction by providing hydrophobic interactions and at least some hydrogen and ionic bonds. Future mutagenesis studies may illuminate the means by which individual residues affect the binding interaction.

Sequence alignment analysis using the DALI database (*45*) revealed that many proteins overlap with either two α-helical structures of LSD1$^{418-522}$ or one helix of linker region$^{293-380}$, suggesting that the helical structure is common to other proteins. Although their sequences do not match with high scores, helical conformations can have structurally similar characteristics. Notably, the trimeric helical features formed by LSD1 tower domain$^{418-522}$ and linker region$^{293-380}$ were not scored as hits by DALI analysis, indicating their unique structure. This analysis suggests that although the helical structure of either LSD1 tower domain$^{418-522}$ or linker region$^{293-380}$ can be used as a structural motif for existing proteins, the trimeric helical structure has less precedent. Thus, small molecules targeting the interaction between LSD1 and CoREST may exhibit high selectivity.

The results of the thermodynamic study of binding between LSD1 and CoREST$^{286-482}$ led us to question the role of full-length CoREST and the effects of other corepressor proteins such

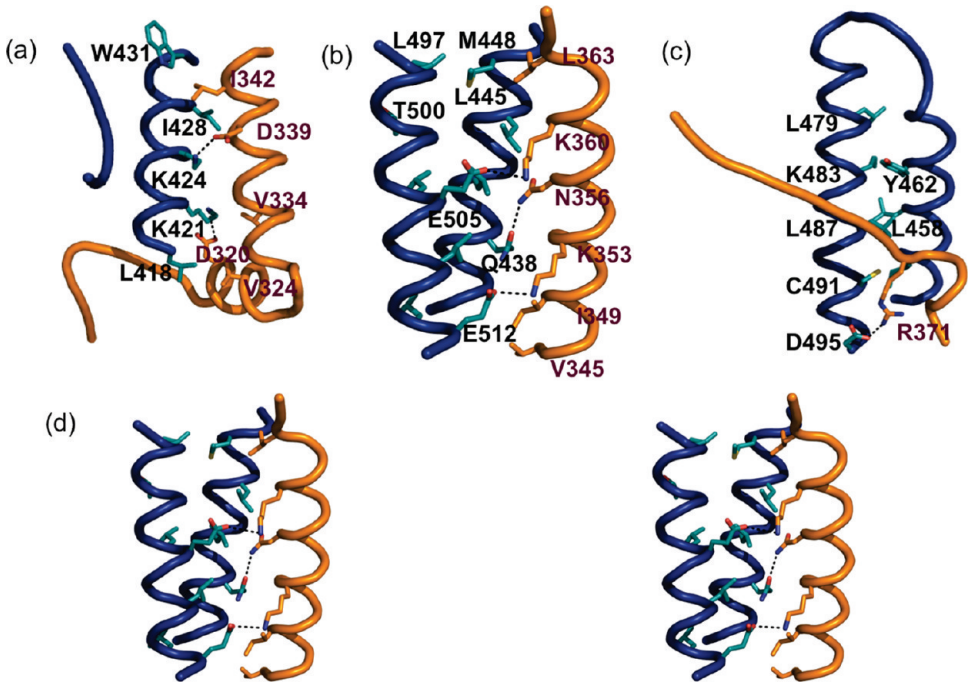

FIGURE 7: Detailed molecular contacts between LSD1 tower region$^{418-522}$ (blue ribbon) and linker region$^{293-380}$ (orange ribbon). Residues are labeled in black for LSD1 and in red for CoREST. Hydrogen bonds are represented by black dashed lines. (a) Interface part I (LSD1 residues 418−432 and 514−522 and CoREST residues 308−344). (b) Interface part II (LSD1 residues 433−450 and 496−513 and CoREST residues 345−365). (c) Interface part III (LSD1 residues 451−495 and CoREST residues 366−380). (d) Stereoview of interface part II. Residues involved in hydrogen bonds in interface part II are shown.

as HDAC 1 and 2 associated with the LSD1−CoREST complex on binding. Previous studies by Yu, Lei, Shi, and Mattevi (*4*−*6*, *21*) demonstrated the importance of C-terminal region of CoREST (residues 286−482) in mediating the demethylase activity of LSD1. In deletion mapping studies, linker region$^{293-380}$ was identified as a putative binding site for LSD1, and SANT2 domain$^{381-450}$ apparently stimulates the demethylation activity of LSD1 by bringing LSD1 to its nucleosomal substrates. Another study by Shiekhattar and co-workers examined the effect of full-length CoREST on the regulation of the activity of LSD1 (*46*). Addition of full-length CoREST increased the demethylase activity of LSD1, and the deletional mapping analysis showed the necessity of both the SANT1 and SANT2 domains for the nucleosomal demethylation, although the stimulatory activity of SANT1 was weak. The SANT1 domain may act as a bridging sequence between LSD1 and its substrates because of the structural similarity with the SANT2 domain. Thus, the SANT1 and SANT2 domains may independently facilitate LSD1-mediated demethylation. Also, the activity of HDAC1 increased upon addition of full-length CoREST because of the role of an ELM2 domain of CoREST that is known to mediate the deacetylase activity of HDAC 1 and 2 (*13*, *47*).

On the basis of these previous studies, full-length CoREST seems to have activity similar to that of truncated CoREST$^{286-482}$. These results let us presume that the ELM2 domain and SANT1 domain of CoREST may be located away from the stalk formed between LSD1 tower domain$^{418-522}$ and linker region$^{293-380}$, and that consequently the binding affinity between LSD1 and full-length CoREST should not be significantly different from the binding affinity obtained between LSD1 and truncated CoREST$^{286-482}$. However, the exact role or function of either domain in binding affinity cannot be rationalized until a crystal structure of LSD1 and full-length CoREST is determined. Whether the presence of HDAC 1 and 2 affects the binding affinity between LSD1 and full-length CoREST may depend on the location of the ELM2 domain in the complex because of its physical association with the ELM2 domain (*13*). Assuming that the N-terminal region of CoREST, including the ELM2 domain and SANT1 domain, is not associated with the binding region of the LSD1−CoREST complex, the presence of HDAC 1 and 2 may not affect the binding affinity significantly as well. However, it is also possible that HDAC 1 and 2 are sufficiently close to the binding region of LSD1 and full-length CoREST because of its spatial occupancy upon binding to the ELM2 domain, resulting in a reduction in binding affinity.

In recent studies (*48*, *49*), LSD2 has been identified as a flavin-dependent histone demethylase, with an enzymatic activity and a substrate specificity profile similar to those of LSD1. Unlike LSD1, however, LSD2 does not contain LSD1 tower domain$^{418-522}$, which is essential for binding to CoREST, but has a CW-type zinc finger domain at its N-terminus between residues 130 and 200. Accordingly, LSD2 is not able to interact with CoREST, distinguishing it from LSD1. The role of the zinc finger domain in LSD2 remains unclear, but we speculate with some degree of confidence that this sequence may facilitate direct binding of LSD2 to nucleosomal DNA.

In summary, our thermodynamic study has verified the tight binding interaction between CoREST, particularly linker region$^{293-380}$, and LSD1, which is both enthalpically and energetically favorable. Future mutational studies will provide valuable insights into key residues involved in the tight binding interaction, supporting our structural analysis. Furthermore, on the basis of the study of binding between LSD1 and CoREST, a study of the binding interaction between HDAC 1 and 2 and the LSD1−CoREST complex should provide a good framework for downregulating epigenetic transcriptional derepression mechanisms associated with cancer progression.

ACKNOWLEDGMENT

We acknowledge the SPR measurement services provided by the Duke Human Vaccine Institute Biomolecular Interaction Analysis Facility under the direction of Dr. S. Munir Alam. We thank Dr. S. Moses Dennison for help with SPR data analyses. We also thank the members of the McCafferty laboratory for their thoughtful insight during the preparation of the manuscript.

SUPPORTING INFORMATION AVAILABLE

Calorimetric titrations of LSD1 with linker region$^{293-380}$ and SANT2 domain$^{381-450}$ of CoREST in 50 mM sodium phophate and 1 mM DTT (pH 7.4) (Figure 1S) and calculation of the change in solvent accessible surface area (ΔASA) using GetArea (*18*) (Table 1S). This material is available free of charge via the Internet at http://pubs.acs.org.

REFERENCES

1. Luger, K. (2003) Structure and dynamic behavior of nucleosomes. *Curr. Opin. Genet. Dev. 13*, 127–135.
2. Wang, G. G., Allis, C. D., and Chi, P. (2007) Chromatin remodeling and cancer, Part I: Covalent histone modifications. *Trends Mol. Med. 13*, 363–372.
3. Yang, M., Culhane, J. C., Szewczuk, L. M., Jalili, P., Ball, H. L., Machius, M., Cole, P. A., and Yu, H. (2007) Structural basis for the inhibition of the LSD1 histone demethylase by the antidepressant trans-2-phenylcyclopropylamine. *Biochemistry 46*, 8058–8065.
4. Yang, M., Gocke, C. B., Luo, X., Borek, D., Tomchick, D. R., Machius, M., Otwinowski, Z., and Yu, H. (2006) Structural basis for CoREST-dependent demethylation of nucleosomes by the human LSD1 histone demethylase. *Mol. Cell 23*, 377–387.
5. Chen, Y., Yang, Y., Wang, F., Wan, K., Yamane, K., Zhang, Y., and Lei, M. (2006) Crystal structure of human histone lysine-specific demethylase 1 (LSD1). *Proc. Natl. Acad. Sci. U.S.A. 103*, 13956–13961.
6. Shi, Y. J., Matson, C., Lan, F., Iwase, S., Baba, T., and Shi, Y. (2005) Regulation of LSD1 histone demethylase activity by its associated factors. *Mol. Cell 19*, 857–864.
7. Yang, M., Culhane, J. C., Szewczuk, L. M., Gocke, C. B., Brautigam, C. A., Tomchick, D. R., Machius, M., Cole, P. A., and Yu, H. (2007) Structural basis of histone demethylation by LSD1 revealed by suicide inactivation. *Nat. Struct. Mol. Biol. 14*, 535–539.
8. Huang, J., Sengupta, R., Espejo, A. B., Lee, M. G., Dorsey, J. A., Richter, M., Oparavil, S., Shiekhattar, R., Bedford, M. T., Jenuwein, T., and Berger, S. L. (2007) p53 is regulated by the lysine demethylase LSD1. *Nature 449*, 105–108.
9. Bradley, C., van der Meer, R., Roodi, N., Yan, H., Chandrasekharan, M. B., Sun, Z., Mernaugh, R. L., and Parl, F. F. (2007) Carcinogen-induced histone alteration in normal human mammary epithelial cells. *Carcinogenesis 28*, 2184–2192.
10. Kahl, P., Gullotti, L., Heukamp, L. C., Wolf, S., Friedrichs, N., Vorreuther, R., Solleder, G., Bastian, P. J., Ellinger, J., Metzger, E., Schule, R., and Buettner, R. (2006) Androgen receptor coactivators lysine-specific histone demethylase 1 and four and a half LIM domain protein 2 predict risk of prostate cancer recurrence. *Cancer Res. 66*, 11341–11347.
11. Lim, S., Janzer, A., Becker, A., Zimmer, A., Schule, R., Buettner, R., and Kirfel, J. (2010) Lysine-specific demethylase 1 (LSD1) is highly expressed in ER-negative breast cancers and a biomarker predicting aggressive biology. *Carcinogenesis 31*, 512–520.
12. Anand, R., and Marmorstein, R. (2007) Structure and mechanism of lysine-specific demethylase enzymes. *J. Biol. Chem. 282*, 35425–35429.
13. You, A., Tong, J. K., Grozinger, C. M., and Schreiber, S. L. (2001) CoREST is an integral component of the CoREST-human histone deacetylase complex. *Proc. Natl. Acad. Sci. U.S.A. 98*, 1454–1458.
14. Shi, Y., Lan, F., Matson, C., Mulligan, P., Whetstine, J. R., Cole, P. A., Casero, R. A., and Shi, Y. (2004) Histone demethylation mediated by the nuclear amine oxidase homolog LSD1. *Cell 119*, 941–953.
15. Schmidt, D. M. Z., and McCafferty, D. G. (2007) *trans*-2-Phenylcyclopropylamine is a mechanism-based inactivator of the histone demethylase LSD1. *Biochemistry 46*, 4408–4416.
16. Gaweska, H., Pozzi, M. H., Schmidt, D. M. Z., McCafferty, D. G., and Fitzpatrick, P. F. (2009) Use of pH and kinetic isotope effects to establish chemistry as rate-limiting in oxidation of a peptide substrate by LSD1. *Biochemistry 48*, 5440–5445.
17. Forneris, F., Binda, C., Vanoni, M. A., Battaglioli, E., and Mattevi, A. (2005) Human histone demethylase LSD1 reads the histone code. *J. Biol. Chem. 280*, 41360–41365.
18. Fraczkiewics, R., and Braun, W. (1998) Exact and efficient analytical calculation of the accessible surface areas and their gradients for macromolecules. *J. Comput. Chem. 19*, 319–333.
19. Davis, F. P., and Sali, A. (2005) PIBASE: A comprehensive database of structurally defined protein interfaces. *Bioinformatics 21*, 1901–1907.
20. Krissinei, E., and Henric, K. (2007) Inference of macromolecular assemblies from crystalline state. *J. Mol. Biol. 372*, 774–797.
21. Forneris, F., Binda, C., Adamo, A., Battaglioli, E., and Mattevi, A. (2007) Structural basis of LSD1-CoREST selectivity in histone H3 recognition. *J. Biol. Chem. 282*, 20070–20074.
22. Lundquist, J. J., and Toone, E. J. (2002) The cluster glycoside effect. *Chem. Rev. 102*, 555–578.
23. Christensen, T., and Toone, E. J. (2003) Calorimetric evaluation of protein-carbohydrate affinities. *Methods Enzymol. 362*, 486–504.
24. Christensen, T., Gooden, D. M., Kung, J. E., and Toone, E. J. (2003) Additivity and the physical basis of multivalency effects: A thermodynamic investigation of the calcium EDTA interaction. *J. Am. Chem. Soc. 125*, 7357–7366.
25. Velazquez-Campoy, A., Ohtaka, H., Nezami, A., Muzammil, S., and Freire, E. (2004) Isothermal titration calorimetry. Current Protocols in Cell Biology, Chapter 17, Unit 17.18, Wiley, New York.
26. Doyle, M. L. (2001) Titration microcalorimetry. Current Protocols in Protein Science, Chapter 20, Unit 20.24, Wiley, New York.
27. Sturtevant, J. M. (1977) Heat capacity and entropy changes in processes involving proteins. *Proc. Natl. Acad. Sci. U.S.A. 74*, 2236–2240.
28. Stites, W. E. (1997) Protein-Protein Interactions: Interface Structure, Binding Thermodynamics, and Mutational Analysis. *Chem. Rev. 97*, 1233–1250.
29. Perozzo, R., Folkers, G., and Scapozza, L. (2004) Thermodynamics of protein-ligand interactions: History, presence, and future aspects. *J. Recept. Signal Transduction Res. 24*, 1–52.
30. Pierce, M. M., Raman, C. S., and Nall, B. T. (1999) Isothermal titration calorimetry of protein-protein interactions. *Methods 19*, 213–221.
31. Frederick, K. K., Marlow, M. S., Valentine, K. G., and Wand, A. J. (2007) Conformational entropy in molecular recognition by proteins. *Nature 448*, 325–329.
32. Lee, B., and Richards, F. M. (1971) The interpretation of protein structures: Estimation of static accessibility. *J. Mol. Biol. 55*, 379–400.
33. Nautiyal, S., and Alber, T. (1999) Crystal structure of a designed, thermostable, heterotrimeric coiled coil. *Protein Sci. 8*, 84–90.
34. Wilson, I. A., Skehel, J. J., and Wiley, D. C. (1981) Structure of the haemagglutinin membrane glycoprotein of influenza virus at 3 Å resolution. *Nature 289*, 366–373.
35. Weis, W. I., Drickamer, K., and Hendrickson, W. A. (1994) Trimeric structure of a C-type mannose-binding protein. *Structure 2*, 1227–1240.
36. Nomizu, M., Utani, A., Beck, K., Otaka, A., Roller, P., and Yamada, Y. (1996) Mechanism of laminin chain assembly into a triple-stranded coiled-coil structure. *Biochemistry 35*, 2885–2893.
37. Eckert, D. M., Malashkevich, V. N., and Kim, P. S. (1998) Crystal structure of GCN4-pIQI, a trimeric coiled coil with buried polar residues. *J. Mol. Biol. 284*, 859–865.
38. Ogihara, N. L., Weiss, M. S., Degrado, W. F., and Eisenberg, D. (1997) The crystal structure of the designed trimeric coiled coil coil-V_aL_d: Implications for engineering crystals and supramolecular assemblies. *Protein Sci. 6*, 80–88.
39. Grigoryan, G., and Keating, A. E. (2008) Structural specificity in coiled-coil interactions. *Curr. Opin. Struct. Biol. 18*, 477–483.
40. Lupas, A. N., and Gruber, M. (2005) The structure of α-helical coiled coils. *Adv. Protein Chem. 70*, 37–78.
41. Lupas, A. N. (1996) Coiled coils: New structures and new functions. *Trends Biochem. Sci. 21*, 375–382.
42. Burkhard, P., Stetefeld, J., and Strelkov, S. V. (2001) Coiled coils: A highly versatile protein folding motif. *Trends Cell Biol. 11*, 82–88.
43. Knappenberger, J. A., Smith, J. E., Thorpe, S. H., Zitzewitz, J. A., and Matthews, C. R. (2002) A buried polar residue in the hydrophobic interface of the coiled-coil peptide, GCN4-p1, plays a thermodynamic, not a kinetic role in folding. *J. Mol. Biol. 321*, 1–6.
44. Hendsch, Z. S., and Tidor, B. (1994) Do salt bridges stabilize proteins? A continuum electrostatic analysis. *Protein Sci. 3*, 211–266.

45. Holm, L., and Rosenstrom, P. (2010) Dali Server: Conservation mapping in 3D. *Nucleic Acids Res. 38*, W545–W549.
46. Lee, M. G., Wynder, C., Cooch, N., and Shiekhattar, R. (2005) An essential role for CoREST in nucleosomal histone 3 lysine 4 demethylation. *Nature 437*, 432–435.
47. Ding, Z., Gillespie, L. L., and Paterno, G. D. (2003) Human MI-ER1 α and β function as transcriptional repressors by recruitment of histone deacetylase 1 to their conserved ELM2 domain. *Mol. Cell. Biol. 23*, 250–258.
48. Karytinos, A., Forneris, F., Profumo, A., Ciossani, G., Battaglioli, E., Binda, C., and Mattevi, A. (2009) A novel mammalian flavin-dependent histone demethylase. *J. Biol. Chem. 284*, 17775–17782.
49. Binda, C., Valente, S., Romanenghi, M., Pilotto, S., Cirilli, R., Karytinos, A., Ciossani, G., Botrugno, O. A., Forneris, F., Tardugno, M., Edmondson, D. E., Minucci, S., Mattevi, A., and Mai, A. (2010) Biochemical, structural, and biological evaluation of tranylcypromine derivatives as inhibitors of histone demethylases LSD1 and LSD2. *J. Am. Chem. Soc. 132*, 6827–6833.